Analysis of Disruption Scenarios and Their Possible Mitigation in ITER

M. Sugihara[1], V. Lukash[2], Y. Kawano[3], R. Khayrutdinov[4], N. Miki[3], A. Mineev[5], J. Ohmori[3], H. Ohwaki[6], D. Humphreys[7], A. Hyatt[7], V. Riccardo[8], D. Whyte[9], V. Zhogolev[2], P. Barabaschi[10], Yu. Gribov[1], K. Ioki[10], M. Shimada[1]

[1] *ITER IT, Naka JWS, Naka, Ibaraki, Japan,* [2] *Kurchatov Institute, Russian Federation,*
[3] *JAERI, Naka, Ibaraki, Japan,* [4] *TRINITI, Troitsk, Russian Federation,*
[5] *Efremov Scientific Res. Institute, Russian Federation,* [6] *Keio Univ. Yokohama, Japan,*
[7] *General Atomics, San Diego, USA,* [8] *EURATOM/UKAEA Culham, Oxford, UK*
[9] *Univ. Wisconsin, Madison, USA,* [10] *ITER IT, Garching JWS, Garching, Germany*
e-mail address of the main author; sugiham@itergps.naka.jaeri.go.jp

Abstract   Database analyses have been carried out to derive physics guidelines for the shortest current quench time and their waveforms as well as the product of halo fraction with toroidal peaking factor arising from disruptions in ITER. Several representative disruption scenarios are specified. Disruption simulations with the DINA code and electromagnetic load (EM) analyses with 3D finite element method (FEM) code are performed for these scenarios. Reasonable margins are confirmed in the forces on in-vessel components due to induced eddy and halo currents for these representative scenarios. It is noted that an increase in the current decay time by a factor of *1.5-2* can reduce the force due to eddy currents significantly at the expense of small increase of halo currents. This condition can be realized by injection of $(1-2)\times10^{24}$ atoms of neon without generating runaway electrons. In the massive injection scheme, the response time can be very fast, and the mitigation for only a small fraction of the total number of disruptions ($\leq$ *(3-4)*%) is missed, while the force on the gas inlet valve becomes high ($\geq$*300 kg*). In the moderate injection case, the response time is rather slow ($\geq$*100 ms*) and the mitigation for a substantial fraction of the total number of disruptions *(40-50)*% is missed, while the force on the inlet valve can be easily handled.

1. Introduction

Examinations of EM load under various disruption conditions expected in ITER are essential to check the robustness of the design against disruptions. Robustness of the vacuum vessel and large in-vessel components, such as the blanket modules (BM) and divertor cassette are particularly important, since they are directly linked with the protection of machine against damage. For this purpose, a proper specification of the representative scenarios based on a detailed assessment of the database is essential [1]. Of particular importance for EM load considerations are the shortest current quench time and product of maximum halo current fraction ($I_{h,max}/I_{p0}$) with toroidal peaking factor (*TPF*), $f_h \equiv (I_{h,max}/I_{p0}) \times TPF$. The waveform of the current quench may also be important. Even if a reasonable margin is confirmed for these representative scenarios, disruption mitigation is still highly desirable to further increase the margin against various uncertainties in plasma behavior. In addition to the EM load, the thermal load on the divertor and first wall during thermal quench and runaway electrons should also be mitigated.

Among the mitigation techniques that have been proposed, massive [2] and moderate [3] noble gas injection techniques are the most promising. A perfect mitigation technique, however, has not yet been established. In fact, a large localized thermal load on the wall in the massive injection technique and deteriorated mitigation success rate due to slow response in the case of moderate injection technique, need further investigation. Nevertheless, both techniques provide a sound basis for the mitigation of EM load and runaway electron generations, which is of primary importance in ensuring the protection of the machine against disruptions. To this end, the key point is to specify the optimum species, amount of impurity and rate of injection. It is also important to assess the mitigation success or missed rate in ITER with these techniques. Here, mitigation success (missed) rates are defined as the ratio of the number of disruptive discharges which are successfully (not successfully) mitigated to the

total number of disruptive discharges, respectively. This assessment can be performed with use of sophisticated disruption prediction methods, such as a neural network system, applied to the possible mitigation scenarios. The success rate is closely linked to the gas pressure and the resulting force on the gas inlet valve through the response speed of the gas injection/penetration.

In this paper, we will first derive a guideline for the shortest current quench time and their waveforms as well as the maximum f_h expected in ITER through database analyses. Based on these guidelines, we will specify several representative disruption scenarios. We will then simulate the plasma behavior and analyze EM load for these scenarios to evaluate the margin in the force acting on the BMs. The optimum species, amount of impurity and rate of injection to mitigate the EM load and runaway generation are specified. Finally, an initial assessment of the mitigation success rate is performed with an application of a neural network prediction technique. The trade-off between success rate and gas pressure will also be examined.

2. Database Analyses for Current Quench Time, Waveform and Halo Current

In this section, we will derive a guideline for a possible shortest current quench time and maximum f_h expected in ITER through a database analyses. As for current quench waveforms, generic characteristics are difficult to identify due to the diversity in disruptions. In the International Disruption Database (IDD) prepared for the ITER physics basis (IPB) [1], which is the most comprehensive scalar database for current quench time presently available, quench times derived from the average current quench rate between some time interval, or the maximum current quench rate, are archived from major tokamaks. Most simply, a linear waveform derived from this average rate can be used for EM load analyses assuming that the average flux change due to current quench will represent a global feature of the EM load on relatively large components such as BMs. In addition, analyses based on more detailed waveforms are also necessary to check the robustness of the design. Thus, we examine the waveforms for the disruptions with the shortest quench time in several machines.

Figure 1 shows current quench times normalized by the poloidal cross-section area ($\Delta t/S$) for major tokamaks taken from IDD. Here Δt is evaluated from the average quench rate between 80% and 20% of the initial plasma current I_{p0}, except for DIII-D and JET, for which the quench rates are evaluated between (90-10)% and (100-40)%, respectively [1]. In JET,
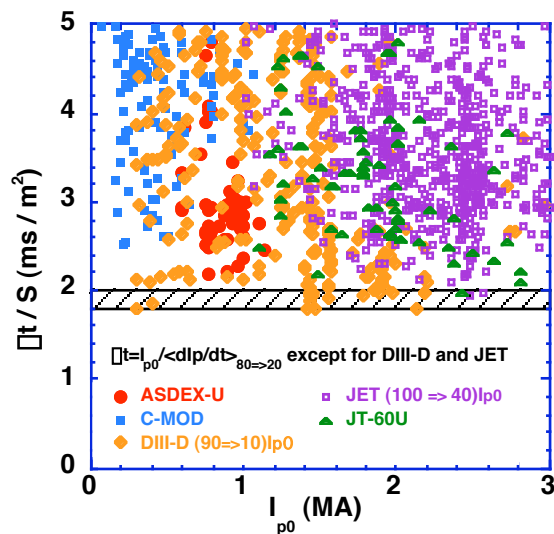

Fig. 1 Current quench time normalized by the poloidal cross-section area vs. initial plasma current for major tokamaks.
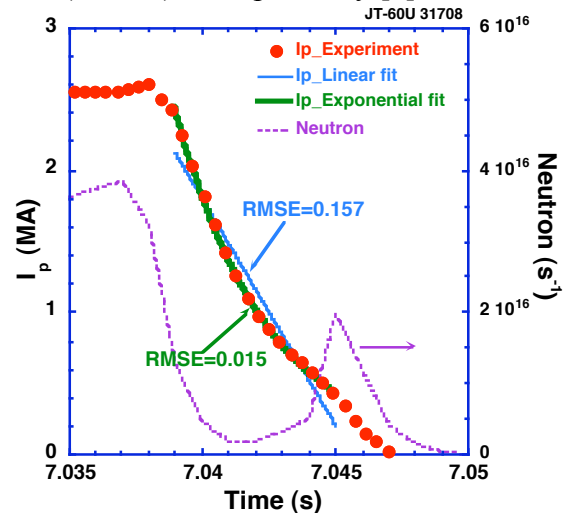
Fig. 2 Fastest quench discharge in JT-60U and its fitting by an exponential waveform. Dotted line shows a photo-neutron rate.

runaway electrons significantly distort the average quench rate and it is shown that $\Delta t(80\text{-}20) > \Delta t(100\text{-}40)$ when compared for the same plasma pulse [5]. From Fig. 1, a minimum ($\Delta t/S$) is $\approx (1.8\text{-}2)\ ms/m^2$, which corresponds to $\approx 40\ ms$ quench time. Thus, the linear waveform with this quench time can be a simple choice for one of the representative scenarios in ITER.

More detailed examinations of the waveform were performed for the fastest current quench disruptions in JET and JT-60U by an exponential fitting. It was found that the waveform can be well fitted by an exponential curve in many of the disruptions with the shortest quench time [4, 5]. Fig. 2 shows one of the fastest quench disruptions in JT-60U and its fitting by an exponential waveform which gives a time constant normalized by the poloidal cross-section $\tau/S \approx 1.2\ ms/m^2$. These fast quench disruptions tend to be associated with the runaway or super thermal electrons due to large induced voltage. In practice, in JT-60U experiments, photo-neutrons are observed for the fast quench case as shown by dotted line in Fig. 2, whereas no photo-neutrons were observed for the slow quench [6]. This tendency is also observed in JET [5], which is considered as a physical background for the observation of $\Delta t(80\text{-}20) > \Delta t(100\text{-}40)$. Since detailed data for the waveform are not available from all machines at present, we will use somewhat simplified specification of τ in ITER for the case of exponential waveform. Namely, we will use that of the exponential curve, which passes through 80% and 20% of I_{p0} for the shortest linear waveform expected in ITER. This provides $\tau \approx 18\ ms$ in ITER. In this paper, we will perform EM load analyses of the BMs using both linear and exponential waveforms as typical current quench waveforms. Examinations of the exponential waveform are especially important for smaller components such as the ICRF antenna and the first wall with time constants shorter than that of BMs. However, these analyses are not discussed in this paper, since we will concentrate on relatively large components, which are critical for the protection of the machine.

Previous experimental data for *TPF* as a function of maximum poloidal halo fraction $I_{h,max}/I_{p0}$ have been summarized in IPB [1]. Figure 3 shows an updated summary of the database with addition of recent experimental data from MAST, JET and JT-60U [7, 8, 9]. This summary confirms the previous conclusion that the maximum $f_h \approx 0.7$. A large poloidal

halo current is driven when the plasma current decays slowly, since the edge safety factor reduces significantly under this condition. In the ITER application, the maximum $I_{h,max}/I_{p0}$ is evaluated in VDE with slow current quench with a simulation code, which is ≈ 0.44 as shown later. Then, *TPF* is evaluated from $0.7/(I_{h,max}/I_{p0})$ and the resulting *TPF* (≈ 1.6) is also applied to disruptions and VDEs with fast current quench. This assumption may somewhat overestimate f_h for fast quench disruptions when compared with JET results, where much stronger reduction of f_h is observed for the VDEs with fast current quench [8].
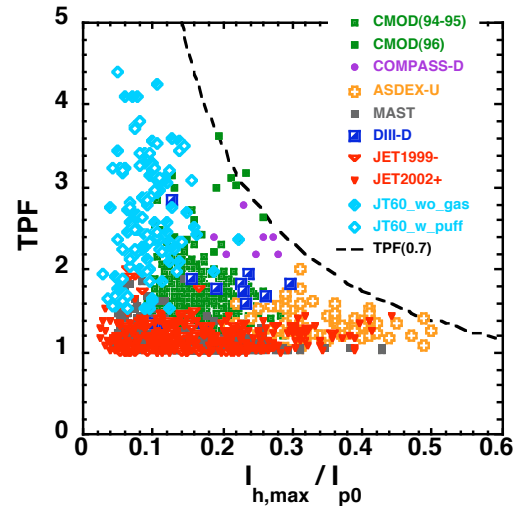

Fig. 3 TPF as a function of maximum poloidal halo current fraction.

3. Analyses of Representative Disruption Scenarios and the Associated EM Load

Based on the database analyses in the previous section, several representative disruption scenarios can be considered. They are summarized in Table I together with other physics assumptions for the simulation, which are mainly taken from Ref. [1]. Although

representative scenarios are numerous when all of the possible combinations are considered, examinations of, at least, these scenarios and EM load analyses are necessary to check the robustness of the design against possible disruption cases.

Representative scenarios Physics guidelines	Major Disruptions (MD)	Down and upward VDE with fast and slow current quench
1. Current quench waveform and time (Fast current quench case)	Linear 40ms and Exponential 18 ms	⇐
2. Thermal quench time duration	Beta drop : 1 ms j flattening : ≈ 3 ms	⇐
3. Surface q value at thermal quench	3	1.5 – 2 [10]
4. Beta drop during thermal quench	≈ 0.72 - 0.75	≈ 0.75 - 0.4
5. Change of li during thermal quench	0.15 - 0.2	⇐
6. $f_h \equiv (I_{h,max}/I_{p0}) \times TPF$ for VDE with slow current quench case		0.7 for slow downward VDE

Table I Representative disruption scenarios and physics assumptions

Numerical simulations are performed with the DINA code [11] for these representative scenarios to evaluate the detailed plasma behavior during major disruptions (MD) and VDEs. The DINA code solves the evolution of 2D plasma equilibrium on closed and open magnetic surfaces together with external circuits (PF coils and surrounding conducting structures). The PF coils are short-circuited and the vacuum vessel is modeled by small sized passive toroidal conductors. Each toroidal row of BMs is modeled by two pairs of toroidally connected plates (inside/outside, top/bottom). They are also connected poloidally with each other at one toroidal location to form a twin-loop, so that the net toroidal current is forced to be zero. Divertor modules are not modeled in the calculation. EM load analyses are performed with a 3D FEM code using the time behavior of the toroidal current density of the plasma column evaluated with the DINA code. Among the representative scenarios, it is shown that one of the most severe EM loads is associated with the disruption when the plasma moves toward the X-point (downward VDE) as expected from the magnetic equilibrium configuration. Consequently, in this paper, we will concentrate on the EM load analyses for this case.
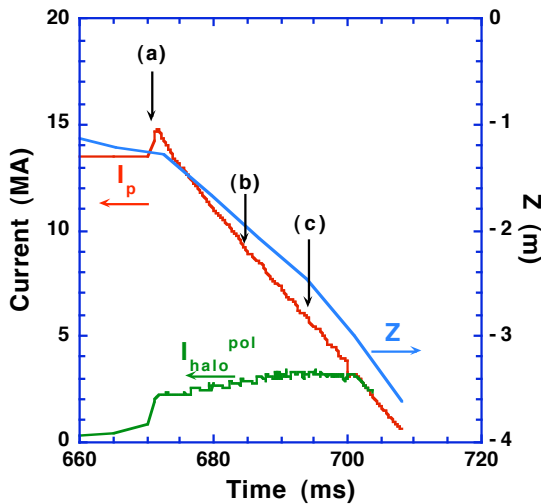

Fig. 4 Time evolutions of plasma current, vertical position and poloidal halo current for downward VDE with linear 40 ms quench.
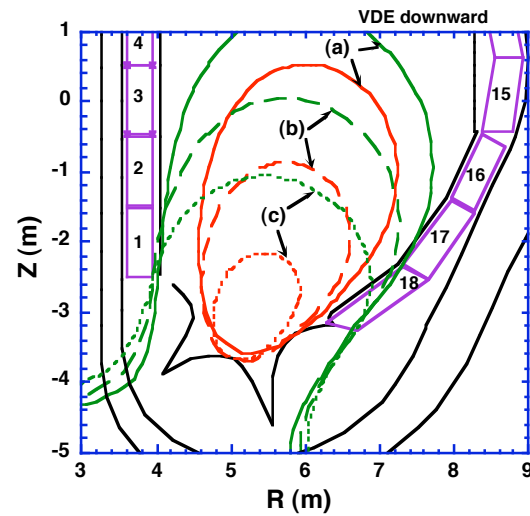
Fig. 5 Time evolution of plasma (LCFS) and halo boundaries for the case of Fig. 4 at three time points (a), (b) and (c).

Figure 4 shows the time evolution of plasma current, vertical position and poloidal halo current for a downward VDE with a linear 40 ms current quench time. Figure 5 shows three time slices of plasma (LCFS) and halo boundaries for this case at (a), (b) and (c) in Fig. 4. Some perturbations or failure of vertical position control are modeled with a small downward impulse at $t = 0$. Plasma moves downward and a thermal quench is assumed to occur when the surface q value reaches *1.5* at $t = 670$ *ms* shown by (a) in the figure.

EM load analyses have been carried out for this case. The BMs are connected to the vacuum vessel through key structures and flexible supports. The key structure restrains the displacement of the module parallel to the vacuum vessel wall reacting the poloidal and toroidal forces and the radial moment. The flexible support reacts to the loads in the radial direction while being compliant in the other directions. Consequently, vertical (poloidal) forces both due to eddy and halo currents are superimposed on the key. Figure 6 shows the time evolution of forces due to both currents and their total on the key of Nr. 1 BM (the inner lowest one as shown in Fig. 5). The *TPF=1.6* is used to evaluate the local maximum force due to the halo current in Fig. 6. The time evolution of the halo current path is obtained by the DINA code calculation, and it is found that the fraction of halo current flowing into the Nr. 1 BM ($f_1 \equiv I_{halo}(Nr.1)/I_{halo,total}$) is always less than *0.5*. Thus, $f_1=0.5$ is assumed during the whole current quench phase to keep some margin against the uncertainty of the plasma behavior. It is seen that a reasonable margin between the design target (dashed line in Fig. 6) and the total force can be maintained. Similarly, a reasonable margin can also be maintained for other BMs as well as for the flexible supports. Simulations with the DINA code and EM load analyses are performed for all of the representative scenarios listed in Table I. For all of the scenarios, the margins are larger or comparable with the downward VDE case. In particular, the maximum EM load for each BM for the exponential waveform with time constant of *18 ms* and the linear waveform with *40 ms* quench time are very similar. This feature can be anticipated by the fact that *Δt(80-20)* for the exponential waveform is exactly same as that for the linear waveform, so that EM loads on large components, e.g., BMs, might be very similar.

Although the present margins are reasonable, more margin would be highly desirable to further increase the robustness of the machine against various uncertainties of the plasma behavior during disruptions. It is seen from Fig. 6 that the maximum EM load (margin) can be significantly reduced (increased) if the force due to eddy current is significantly reduced while the force due to halo current increases only slightly. Figure 7 shows the $I_{h,max}$ (squares) evaluated with the DINA code for different current quench times after a thermal quench and
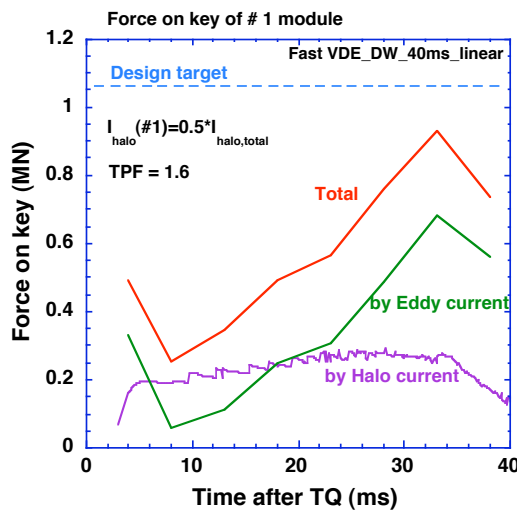

Fig. 6 Time evolutions of forces due to both currents and their total on the key of Nr. 1 blanket module
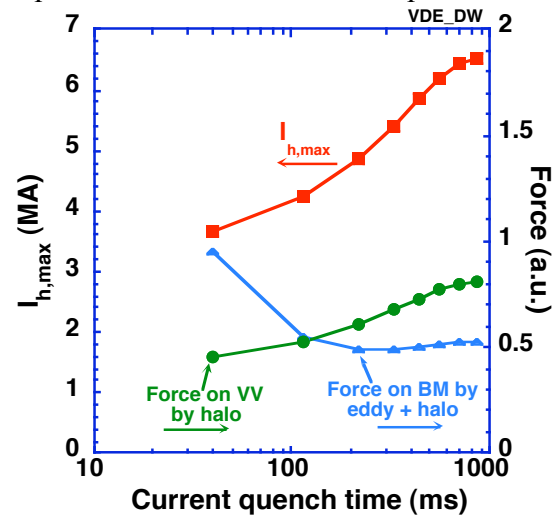
Fig. 7 $I_{h,max}$ (squares) for different current quench times after thermal quench and the associated force on the vacuum vessel (circles).

the associated force on the vacuum vessel (circles). The total force on the key of the Nr. 1 BM due to both eddy and halo currents (triangles) is also shown. It is seen from Fig. 7 that the increase of the current quench time from *40 ms* by only a factor of *1.5-2* significantly reduces the force due to eddy current (*25-50%*) whereas the increase in the force due to halo current is relatively small (*10-15%*).

4. Choice of Impurity Species and Amount for Disruption Mitigation

The mitigation of the EM load envisaged in the previous section can be realized using a disruption mitigation technique, in which either a massive or moderate impurity gas injection are provided. The species, amount of impurity and rate of injection have to be appropriately selected. These mitigation techniques have been extensively studied for the last few years [2, 3]. In addition to the mitigation of EM load, suppression of runaway electron generation is another important goal. The effectiveness of mitigation of the thermal load on the divertor and first wall due to the thermal quench is still not clear. This is due to the uncertainty of radiation collapse time duration and localization for the case of massive injection and comparatively slow response of radiation energy release for the case of moderate injection case. Thus, in the present paper, we will concentrate on the mitigation of the EM load and runaway electron generation.

In order to examine the current quench time and runaway generation, a 0D time dependent code has been developed to calculate the impurity rate equations for each ionization state and the associated radiation loss [12]. These are coupled with a set of equations for plasma power balance, plasma circuit, Dreicer and avalanche runaway electron generation [13]. Coulomb collision as well as elastic and inelastic collisions of electrons with neutrals are taken into account to evaluate the plasma resistivity under high density and low temperature conditions. Figure 8 shows the L/R time constant, $\tau_{L/R}$, calculated with this code for neon (squares), carbon (circles) and argon (triangles) with changing the impurity density, respectively. The range of impurity density for runaway generation is shown for neon. For carbon and argon, they are shown with dashed curves. It is seen that $\tau_{L/R}$ for neon is generally longer than carbon (unmitigated) case, and for the density range of $n_{Ne}=(1\text{-}2)\times10^{21}m^{-3}$, $\tau_{L/R}$
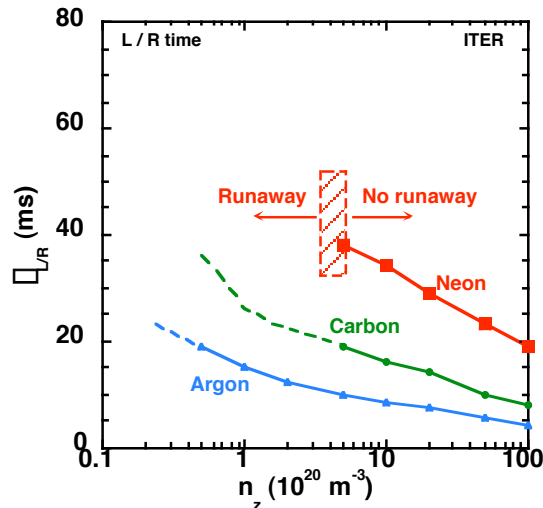

Fig. 8 L/R time constant calculated for neon (squares), carbon (circles) and argon (triangles) vs. impurity density. Boundary of runaway electron generation is shown for neon by hatched region. Dashed lines for carbon and argon show the runaway region.
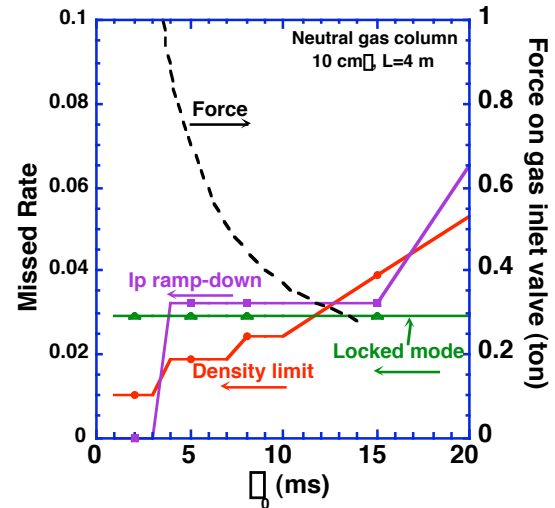
Fig. 9 Force on gas inlet valve vs. τ_0 (dashed lines). Missed rate vs. τ_0 for disruptions triggered by density limit (circles), locked mode (triangles) and high internal inductance during current ramp-down (squares).

$\approx$*30-35 ms*, which is *1.5-2* times longer than the assumed shortest quench time constant of *18 ms* with the exponential waveform employed for the EM load analyses in the previous sections. It is also seen that runaway electrons will not be generated for this range of density.

5. Required Gas Pressure, Response Time and Mitigation Success Rate

To realize the effective mitigation envisaged in the previous section, an appropriate amount of neon, i.e., total $N_{Ne}\approx(1-2)\times10^{24}$ atoms must be injected and these particles must penetrate into the plasma center within a specified time τ_0. The mitigation success rate can be increased if τ_0 is reduced. This is a great benefit for the massive injection technique. On the other hand, a high pressure gas reservoir is needed, which makes the design of the gas inlet valve difficult due to the required fast response under a large force. These features are opposite in the case of a moderate injection technique. Here we will make an initial assessment of these issues. First we assume that the required pressure of the neutral gas for penetration into the plasma center is roughly equal to the average plasma pressure ($\overline{P}\approx3\times10^5$ *Pa*). When the pressure of the gas reservoir is high, the neutral gas column can be filled up to $\overline{P}$ in a short time, namely τ_0 can be short. This τ_0 can be evaluated by solving the equation for the pressure increase using the analogy of critical gas flow of the nozzle (i.e., critical flow rate is restricted to those values at the gas inlet valve with Mach number=1) for different pressure of the reservoir P_0. For each P_0, the force acting on the inlet valve F can be evaluated as $F= P_0\times S$, where S is the area of the inlet valve. In Fig. 9, dashed line shows the calculated force as a function of τ_0. Here, the diameter and length of the neutral gas column are assumed *10 cm* and *4 m*, respectively.

To demonstrate how the duration τ_0 is related to the mitigation success (or missed) rate, we will employ a neural network disruption prediction system recently developed based on JT-60U disruption data [14] as an example. One major advantage of this network system is that the prediction success rate can be significantly increased with maintaining the prediction false rate very low (typically $\approx$*2%*). Here, the prediction false rate is defined as the ratio of the number of non-disruptive discharges to which the mitigation is erroneously triggered, to the total number of non-disruptive discharges. In Ref. [14], the prediction success rate is evaluated as a function of the time prior to the disruption onset, which is equivalent to τ_0 in the present definition, for various types of disruptions. The results are shown in Fig. 9 for the disruptions triggered by density limit (circles), locked mode (triangles) and high internal inductance during current ramp-down (squares). The missed rate increases with increasing τ_0, while F decreases significantly.   However, the increase of missed rate is not so significant as long as τ_0 is not so long. In fact, for τ_0=*15 ms* and consequent *F=300 kg*, the missed rates are still *(3-4) %*. In the case of moderate injection technique, it is demonstrated that the plasma current can be terminated without runaway generation by the combined injection of noble gas and hydrogen [3]. In this case, the force on the gas inlet valve is low, while the response time is considerably longer ($\geq$*100 ms*) and accordingly the missed rate increases to *(40-50)%*. Future design selection between massive and moderate injection techniques in ITER will be made considering these trade-off features. In addition, further experimental data of the heat load on the first wall (time duration and localization) due to the enhanced radiation in the massive injection technique and that on the divertor in the moderate injection technique are necessary for this selection. It should also be noted that disruptions at the beta limit cannot be predicted satisfactorily with the algorithm in Ref. [14]. This is also shown based on a different algorithm in Ref. [15], where the success rate cannot be increased without increasing the false rate. Thus, substantial improvement of the algorithm for high beta disruptions is another essential ingredient to mitigate the impacts of disruptions in ITER by any mitigation system.

6. Conclusions

Database analyses are carried out and physics guidelines for the shortest current quench time and their waveforms ($\Delta t \approx 40\ ms$ linear and $\tau \approx 18\ ms$ exponential waveforms), as well as a production of halo fraction with toroidal peaking factor (maximum $f_h \approx 0.7$) expected in ITER, are derived. Based on these analyses, several representative disruption scenarios are specified. Disruption simulations with the DINA code and EM load analyses with the 3D FEM code are performed for these scenarios. Reasonable margins in the forces on the in-vessel components due to induced eddy and halo currents are confirmed for all of the representative scenarios. It is noticed that with the increase of the current decay time by a factor of *1.5-2*, the force on the BMs due to eddy currents can be significantly reduced at the expense of only moderate increase of halo currents. Disruption mitigation techniques both by massive and moderate impurity gas injection techniques are examined and it is shown that this condition can be realized by the injection of *(1-2)×10^{24}* atoms of neon without generating runaway electrons. In the massive injection technique, the response time can be very fast, with which the mitigation missed rate can be small ($\leq$ *(3-4)%*) while the force acting on the gas inlet valve becomes high ($\geq 300\ kg$). In the moderate injection technique, the response time is rather slow ($\geq 100\ ms$) and accordingly the missed rate increases to (*40-50*)%, while the force on the gas inlet valve is low. More detailed trade-off studies and optimization are necessary for these mitigation techniques to incorporate these techniques into the design. In addition, further experimental data of the heat load on the first wall (time duration and localization) due to the enhanced radiation in the massive injection technique, and heat load on the divertor in the moderate injection technique, are needed.

Acknowledgements

References
[1] ITER Physics Basis, Nucl. Fusion **39** (1999) 2137.
[2] Whyte, D., J. Nucl. Material. **313-316** (2003) 1239.
[3] Bakhtiari, M., et al., Nucl. Fusion **42** (2002) 1197.
[4] Sugihara, M., et al., J. Plasma Fusion Science **79** (2003) 706.
[5] Riccardo, V., et al., submitted to Plasma Phys. Control. Fusion.
[6] Sugihara, M., et al., 30th EPS, St. Petersburg (2003), P-2.139.
[7] Riccardo, V., Plasma Phys. Control. Fusion **45** (2003) A269.
[8] Riccardo, V., Plasma Phys. Control. Fusion **46** (2004) 925.
[9] Neyatani, Y., et al Nucl. Fusion **39** (1999) 559.
[10] Sugihara, M., et al., Plasma Phys. Control. Fusion **46** (2004) 1581.
[11] Khayrutdinov, R.R. et al, J. Comp. Physics **109** (1993) 193.
[12] Mineev, A., et al., ITER Task Report (to be published).
[13] Rosenbluth, M., et al., Nucl. Fusion **37** (1997) 1355.
[14] Yoshino, R., Nucl. Fusion **43** (2003) 1771.
[15] Wroblewski, D., et al., Nucl. Fusion **37** (1997) 725.